



The effect of A-site substitution by Sr, Mg and Ce on the catalytic performance of LaMnO_3 catalysts for the oxidation of vinyl chloride emission

Chuanhui Zhang^{a,b}, Wenchao Hua^a, Chao Wang^a, Yanglong Guo^{a,*}, Yun Guo^a, Guanzhong Lu^a, Alexandre Baylet^b, Anne Giroir-Fendler^{b,**}

^a Key Laboratory for Advanced Materials and Research Institute of Industrial Catalysis, East China University of Science and Technology, Shanghai 200237, PR China

^b Université Lyon 1, CNRS, UMR 5256, IRCELYON, Institut de recherches sur la catalyse et l'environnement de Lyon, 2 avenue Albert Einstein, 69626 Villeurbanne Cedex, France

ARTICLE INFO

Article history:

Received 26 October 2012

Received in revised form 4 January 2013

Accepted 7 January 2013

Available online 24 January 2013

Keywords:

Vinyl chloride

Catalytic oxidation

Perovskite catalyst

Reducibility

Adsorbed oxygen

ABSTRACT

Catalytic oxidation of vinyl chloride (VC) emission was carried out over LaMnO_3 and $\text{La}_{0.8}\text{A}_{0.2}\text{MnO}_3$ (A = Sr, Mg and Ce) perovskite oxides synthesized via co-precipitation method. Numerous characterization techniques were performed to investigate the relationship between the catalytic performance and its physicochemical properties. It was found that the partial substitution of lanthanum by cerium and magnesium had a positive effect on the catalytic performance for VC oxidation, whereas strontium involved a negative effect. Under the reaction conditions (VC concentration = 1000 ppm, GHSV = $15,000 \text{ h}^{-1}$), the overall catalyst ranking in terms of the catalytic activity from the best to the worst performance was $\text{La}_{0.8}\text{Ce}_{0.2}\text{MnO}_3 > \text{La}_{0.8}\text{Mg}_{0.2}\text{MnO}_3 > \text{LaMnO}_3 > \text{La}_{0.8}\text{Sr}_{0.2}\text{MnO}_3$ with regard to the temperature of T_{50} and T_{90} . The Ce-doped perovskite catalyst showed the optimum catalytic performance due to its higher specific surface area and its ability to promote the low-temperature reducibility. Moreover, as the active species, the increased surface adsorbed oxygen was also responsible for the enhancement of the catalytic performance.

© 2013 Elsevier B.V. All rights reserved.

1. Introduction

As the main reactant in the industrial production process of polyvinyl chloride (PVC), large amounts of vinyl chloride (VC) emission with a high concentration up to 1–2% are released. The untreated exhaust gas makes wide range of pollution to the atmospheric environment and becomes a hidden trouble to the public health. Nowadays, direct incineration remains the most wide-applied pathway in the field of industrial emissions abatement. However, compared with direct incineration, catalytic oxidation can be operated at relatively lower temperature, lower level of energy consumption and exhibits higher purification efficiency. Thus, it is considered as an efficient and potential technology in eliminating chlorinated volatile organic compounds (CVOs) [1,2].

Among the catalysts used for the catalytic oxidation of CVOs, zeolites, supported noble metals and transition metal oxides have been commonly investigated by researchers [3–5]. Although zeolites present high specific surface areas and variable pore structures, they exhibit relatively poor activity at low temperature.

Precious metal based catalysts are highly active but their expensive cost and catalytic deactivation caused by Cl poisoning are the main problems limiting their applications. Among the transition metal oxides, perovskite-type oxides (with the general formula ABO_3) have attracted much attention due to their low cost, relatively high catalytic activity and good thermal stability. Moreover, they are usually studied as catalysts for numerous VOCs oxidation [6–8]. The most popular perovskites reported for total oxidation of VOCs are the compounds containing rare earth or alkaline earth metals (i.e. La, Pr, Ce, Ba) in the A-site and transition metals (i.e. Co, Ni, Fe, Mn and Cr) in the B-site [9–11]. For example, Levasseur and Kaliaguine [10] prepared a series of AMnO_3 (A = Y, La, Pr, Sm and Dy) catalysts by a reactive grinding method, and investigated the effect of different rare earth metals on the catalytic properties for methanol oxidation. Agarwal and Goswami [12] studied the catalytic oxidation of toluene over LaMO_3 (M = Co, Fe, and Cr) catalysts, finding that LaCoO_3 showed the highest catalytic activity. Additionally, for the perovskite oxides, a modification of redox ability and oxygen defects can be achieved by a partial substitution of other cations with similar oxidation state and ionic radius in the A-site or B-site [13–15]. Luis E. Cadús et al. [16] prepared $\text{La}_{1-x}\text{Ca}_x\text{CoO}_3$ ($x = 0, 0.2, 0.4, 0.5$) perovskite-type oxides by the citrate method and tested their catalytic potentiality for the total oxidation of propane. Results indicated that the partial substitution of La by Ca in the A site of LaCoO_3 improved the catalytic performance for propane

* Corresponding author. Tel.: +86 21 64 25 29 23; fax: +86 21 64 25 29 23.

** Corresponding author. Tel.: +33 4 72 43 15 86; fax: +33 4 72 43 16 95.

E-mail addresses: ylguo@ecust.edu.cn (Y. Guo), anne.giroir-fendler@ircelyon.univ-lyon1.fr (A. Giroir-Fendler).

oxidation. This enhancement was attributed to the increased oxygen vacancies and reductive stoichiometry. In the case of the VOC oxidation over $\text{La}_{1-x}\text{Ce}_x\text{Co}_{1-y}\text{Fe}_y\text{O}_3$ [17], the catalytic activities of Fe-doped catalysts were inferior to the Fe-free counterparts, which was due to a drop in oxygen mobility and B-site cation reducibility. However, in the recent studies for CVOCs oxidation, the majority of catalysts were focused on noble metals and transition metal composite oxides. As one of the promising candidates, perovskite oxides, specifically LaMnO_3 -based catalysts, have obtained little attention in this field.

In our previous work [18], the effect of B-site substitution by Co, Ni and Fe on the catalytic performance of LaMnO_3 catalysts for vinyl chloride oxidation was investigated. A series of $\text{LaB}_{0.2}\text{Mn}_{0.8}\text{O}_3$ ($\text{B}=\text{Co}$, Ni and Fe) catalysts were prepared by the conventional co-precipitation method. The obtained materials exhibited excellent catalytic performance for the total oxidation of vinyl chloride. Ranking the catalyst based on catalytic activity from the highest to the lowest was as follows: $\text{LaNi}_{0.2}\text{Mn}_{0.8}\text{O}_3 > \text{LaCo}_{0.2}\text{Mn}_{0.8}\text{O}_3 > \text{LaFe}_{0.2}\text{Mn}_{0.8}\text{O}_3 > \text{LaMnO}_3$. In order to investigate the effect of A-site substitution on the physicochemical properties and catalytic performance for VC oxidation, we synthesized a series of $\text{La}_{0.8}\text{A}_{0.2}\text{MnO}_3$ ($\text{A}=\text{Sr}$, Mg and Ce) perovskite-type catalysts by adopting the same fabrication strategy.

2. Experimental

2.1. Catalyst preparation

The LaMnO_3 and substituted $\text{La}_{0.8}\text{A}_{0.2}\text{MnO}_3$ ($\text{A}=\text{Sr}$, Mg and Ce) catalysts were prepared by co-precipitation method. To an aqueous solution containing the metal nitrates as the precursors at a desired stoichiometric ratio, $2\text{ mol L}^{-1} - 1\text{ mol L}^{-1}$ $\text{NaOH}-\text{Na}_2\text{CO}_3$ aqueous solution was added dropwise under magnetic stirring until the pH value reached 10. After that, the resulting suspension was aged for 4 h at room temperature, filtered and thoroughly washed with the deionized water. The obtained precipitate was dried at 120°C overnight and calcined at 750°C for 2 h in a muffle furnace, yielding the perovskite structure. To simplify the description, the sample unsubstituted LaMnO_3 and the samples where La was substituted by Sr, Mg and Ce were denoted as LMO, LSMO, LMMO and LCMO, respectively.

2.2. Catalyst characterization

Inductively coupled-plasma atomic emission spectroscopy (ICP-AES) was carried out on a Varian 710-ES instrument in order to determine the chemical compositions of the different perovskites. The powder X-ray diffraction (XRD) patterns were recorded on a Bruker AXS D8 Focus diffractometer using $\text{CuK}\alpha$ radiation (40 kV , 40 mA , $\lambda = 1.5406\text{ \AA}$, scanning rate $= 6^\circ\text{ min}^{-1}$). Nitrogen adsorption at low temperature (77 K) was performed on a Micromeritics ASAP 2020M surface area and porosity analyzer. The specific surface area (SSA) was obtained by Brunauer–Emmett–Teller (BET) method. Temperature programmed reduction of hydrogen (H_2 -TPR) was carried out on a TP-5080 Auto multiple-purpose sorption instrument equipped with a thermal conductivity detector (TCD). 40 mL min^{-1} of the reducing gas mixture composed of $5\text{ vol.}\%$ H_2 diluted in N_2 was passed over the sample (100 mg) placed in a U-shaped quartz reactor. The reactor was heated at a temperature rate of $10^\circ\text{C min}^{-1}$ from room temperature to 900°C and maintained for 20 min at this temperature. The H_2 consumption was quantitatively measured by time integration of the TPR profiles. The TCD signal was calibrated with a commercial CuO sample (SCR, 99.99%). X-ray photoelectron spectroscopy (XPS) was performed on a Thermo ESCALAB 250 spectrometer with a monochromatized

$\text{AlK}\alpha$ X-ray source (1486.6 eV) and a passing energy of 20 eV . The binding energy (BE) was determined by utilizing C 1s of adventitious carbon with the binding energy of 284.8 eV as a reference. XPS spectra were deconvoluted by the curve fitting after the Shirley-type background subtraction.

2.3. Measurement of catalytic activity

The catalytic performance of each sample was measured in a quartz tubular (i.d. = 12 mm) fixed-bed reactor at atmospheric pressure. 500 mg of the catalyst, previously pressed, tableted and sieved into a $40-60$ mesh, was packed in the reactor and the activity evaluation was carried out in the temperature range from 50 to 350°C . Liquefied VC (b.p. = -13.9°C), stored in a stainless steel cylinder, was gasified at room temperature (25°C). The gaseous VC, controlled by a digital mass flowmeter (SeverStar) and set with a flow rate of 0.12 mL min^{-1} , was diluted by air to reach a VC concentration of 1000 ppm . The total flow rate was 120 mL min^{-1} , corresponding to a GHSV of $15,000\text{ h}^{-1}$. A thermocouple was placed in the middle of the catalyst bed to measure the reaction temperature. On-line analysis of gas effluent was performed on a Fuli 9790 gas chromatograph (GC) equipped with a flame ionization detector (FID). Only HCl , CO_2 and H_2O products were detected. No byproducts, such as chlorohydrocarbons and chlorine, were detected, which could be qualitatively identified by INFICON IPC400 quadrupole mass spectrometer. The VC conversion (X_{VC}) was calculated based on the following equation:

$$X_{\text{VC}}(\%) = \frac{[\text{VC}]_{\text{in}} - [\text{VC}]_{\text{out}}}{[\text{VC}]_{\text{in}}} \times 100$$

where $[\text{VC}]_{\text{in}}$ and $[\text{VC}]_{\text{out}}$ were the VC concentrations in the inlet and outlet gas, respectively.

3. Results and discussion

3.1. Physicochemical properties

The crystal structures, chemical compositions and specific surface areas of all samples are summarized in Table 1. The corresponding XRD patterns are shown in Fig. 1. By referring to the standard powder diffraction file (PDF) in the database of the International Centre of Diffraction Data (ICDD), the intense diffraction peaks (at $2\theta = 23.1^\circ$, 32.6° , 40.3° , 47.0° , 53.1° , 58.4° , 68.3° and 77.8°) correlated with those of the $\text{LaMnO}_{3.26}$ structure (JCPDS No. 50-0299), indicating that the perovskite phases corresponding to a rhombohedral symmetry (space group $R-3c$) were obtained. This result was in accordance with those previously reported by Alonso et al. [19] and Song and co-workers [20]. Due to the detection limit of the X-ray diffractometer, no diffraction peaks assignable to the La_2O_3 and/or MnO_x species were observed for all samples. However, a diffraction peak at $2\theta = 28.5^\circ$ was present for the LCMO sample. This peak could be assigned to the characteristic peak of the CeO_2 phase (JCPDS No. 81-0792). The presence of the CeO_2 phase was attributed to the surface enrichment of atomic cerium,

Table 1

Physicochemical properties of LaMnO_3 and $\text{La}_{0.8}\text{A}_{0.2}\text{MnO}_3$ ($\text{A}=\text{Sr}$, Mg and Ce) catalysts.

Samples	Chemical composition ^a	Symmetry ^b	SSA ^c ($\text{m}^2\text{ g}^{-1}$)
LMO	$\text{La}_{1.01}\text{Mn}_{0.99}\text{O}_{3\pm\delta}$	Rhombohedral $R-3c$	17.5
LSMO	$\text{La}_{0.79}\text{Sr}_{0.19}\text{Mn}_{1.02}\text{O}_{3\pm\delta}$	Rhombohedral $R-3c$	16.6
LMMO	$\text{La}_{0.82}\text{Mg}_{0.16}\text{Mn}_{1.02}\text{O}_{3\pm\delta}$	Rhombohedral $R-3c$	30.6
LCMO	$\text{La}_{0.80}\text{Ce}_{0.21-\epsilon}\text{Mn}_{1.00}\text{O}_{3\pm\delta} + \epsilon\text{CeO}_2$	Rhombohedral $R-3c$	35.5

^a Determined by ICP-AES analysis.

^b Determined by XRD patterns (MDI Jade 5.0 program).

^c Measured by N_2 adsorption (BET method).

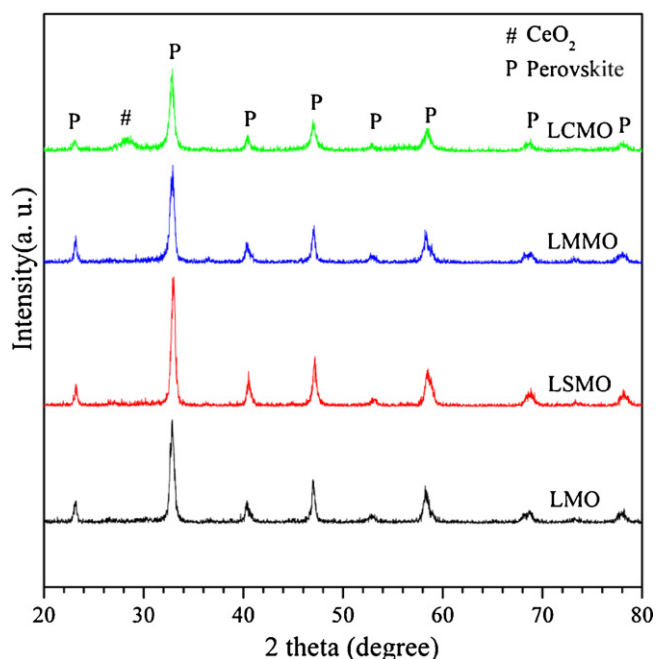


Fig. 1. XRD patterns of LaMnO_3 and $\text{La}_{0.8}\text{A}_{0.2}\text{MnO}_3$ ($\text{A} = \text{Sr, Mg and Ce}$) catalysts.

not being incorporated into the LaMnO_3 perovskite framework during the calcination process. Within experimental error, the element contents of the LMO, LSMO and LCMO samples were fairly close to the theoretical values (Table 1). However, it is important to point out that the experimental magnesium amount was relatively lower than the nominal one for the LMMO sample. Additionally, because of the existence of CeO_2 , the LCMO sample was considered as a multiple oxides containing Ce-doped perovskite and cerium oxide. The results of low temperature N_2 adsorption were also listed in Table 1. Compared to the LMO sample, the SSA values of the LMMO and LCMO samples increased due to the addition of magnesium and cerium. Among all, the LSMO sample had the lowest SSA value, while the LCMO sample had the highest one, $16.6 \text{ m}^2 \text{ g}^{-1}$ and $35.5 \text{ m}^2 \text{ g}^{-1}$, respectively. It has been reported that the cerium oxide synthesized via a coprecipitation route could remain relatively high specific surface area even after an aging at 800°C for 3 h [21]. Thus, the high SSA value of the LCMO sample could be attributed to the contribution of cerium species on this sample.

3.2. Reducibility

For the oxidation catalysts, the reducibility is an important parameter influencing the catalytic activity. In order to investigate the relative reducibility of each sample, the H_2 -TPR experiments of the calcined catalysts were performed. The TPR profiles are shown in Fig. 2 and the H_2 -uptake values owing to each reduction region calculated through the quantitative integration of the separated peaks are listed in Table 2. For all samples, mainly two reduction

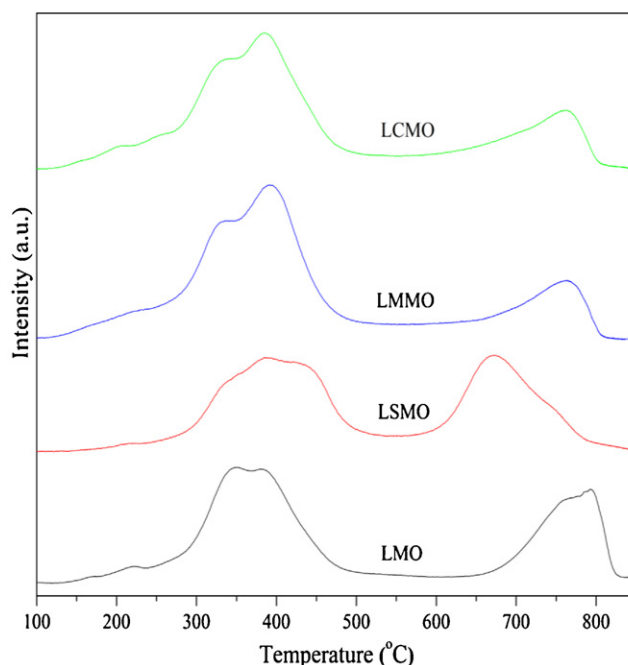


Fig. 2. H_2 -TPR profiles of LaMnO_3 and $\text{La}_{0.8}\text{A}_{0.2}\text{MnO}_3$ ($\text{A} = \text{Sr, Mg and Ce}$) catalysts.

peaks could be observed. The first one was in the low temperature range from 125 to 550°C and the second one was in the high temperature range from 550 to 850°C .

In the low temperature region, a small amount of H_2 consumption occurred below 250°C with a H_2 -uptake of 0.28 , 0.22 , 0.30 and 0.37 mmol g^{-1} for the samples LMO, LSMO, LMMO and LCMO, respectively. It could be attributed to the removal of some adsorbed oxygen species on the surface and could confirm the promotional effect of Ce and Mg substitution on the reducibility of the LaMnO_3 -based catalysts. Large amounts of H_2 consumption was followed by two partially overlapped peaks in the temperature range of 250 – 550°C and the H_2 -uptake was 1.36 , 1.33 , 1.55 and 1.46 mmol g^{-1} for the samples LMO, LSMO, LMMO and LCMO, respectively. The consumed H_2 participated in the reduction process of Mn^{4+} into Mn^{3+} in perovskite structure according to the literatures [22,23]. For the overall low temperature domain, H_2 -TPR results revealed that Mg- and Ce-doped samples had greater H_2 -uptake with a total of 1.85 and 1.83 mmol g^{-1} , respectively, than that of LaMnO_3 with 1.64 mmol g^{-1} . The Sr-doped sample had the lowest value of 1.55 mmol g^{-1} . These results indicated that the low-temperature reducibility of LaMnO_3 catalyst could be improved by the substitution of Mg and Ce, Sr having a negative effect.

In the high temperature region, from 550 to 850°C , one intense peak appeared corresponding to the H_2 -uptake of 0.95 , 1.08 , 0.75 and 0.82 mmol g^{-1} for the pure sample and the Sr, Mg and Ce substituted samples, respectively, which could be correlated with the partial reduction of Mn^{3+} into Mn^{2+} . More specifically for the LCMO sample, due to the existence of CeO_2 species identified by XRD analysis, a reduction of CeO_2 may occur in this region [24,25]. However, as a result of the low cerium concentration and/or overlapped reduction process, it was difficult to obviously identify the peak corresponding to the reduction of Ce^{4+} into Ce^{3+} .

3.3. XPS analysis

In order to investigate the surface element compositions, the manganese oxidation states and the nature of the adsorbed oxygen species, pure LaMnO_3 perovskite and the Sr, Mg, and Ce substituted

Table 2
 H_2 -uptakes of LaMnO_3 and $\text{La}_{0.8}\text{A}_{0.2}\text{MnO}_3$ ($\text{A} = \text{Sr, Mg and Ce}$) catalysts.

Catalyst	H_2 -uptakes ($\text{mmol g}^{-1} \text{ cat.}$)				
	$T^a < 250$	$250 < T^a < 550$	$T^a > 550$	Low-temperature range	Total
LMO	0.28	1.36	0.95	1.64	2.59
LSMO	0.22	1.33	1.08	1.55	2.64
LMMO	0.30	1.55	0.75	1.85	2.60
LCMO	0.37	1.46	0.82	1.83	2.66

^a Temperature ($^\circ\text{C}$).

Table 3
XPS results of LaMnO_3 and $\text{La}_{0.8}\text{A}_{0.2}\text{MnO}_3$ (A = Sr, Mg and Ce) catalysts.

Samples	Surface atomic ratios			Molar ratios ^b	
	La/(La + A + Mn)	Mn/(La + A + Mn)	A/La	Mn ⁴⁺ /Mn	O _β /O
LMO	0.59 (0.50) ^a	0.41 (0.50)	–	0.53	0.41
LSMO	0.51 (0.40)	0.39 (0.50)	0.21 (0.25)	0.48	0.36
LMMO	0.53 (0.40)	0.44 (0.50)	0.07 (0.25)	0.56	0.44
LCMO	0.44 (0.40)	0.37 (0.50)	0.44 (0.25)	0.57	0.47

^a The data in brackets are calculated according to the nominal compositions of LaMnO_3 and $\text{La}_{0.8}\text{A}_{0.2}\text{MnO}_3$ (A = Sr, Mg and Ce) catalysts.

^b Calculated from the corresponding areas of fitted peaks done by XPSPEAK 4.1 with Shirley background.

samples were analyzed by XPS technique. The surface atomic ratios of the La, Mn, Sr, Mg and Ce elements are summarized in Table 3. The surface La/(La + A + Mn) atomic ratios were higher than the nominal values for all samples, indicating that La enrichment occurred on the surface. Similar phenomenon has been reported by other researchers [26,27]. Moreover, for the LCMO sample, the Ce/La surface atomic ratio was much higher than the nominal one, which could be caused by the small amount of CeO_2 identified by XRD analysis.

Fig. 3 shows the Mn 2p_{3/2} and O 1s XPS spectra of the LaMnO_3 and $\text{La}_{0.8}\text{A}_{0.2}\text{MnO}_3$ (A = Sr, Mg and Ce) samples and the Ce 3d XPS spectrum of the LCMO sample. As seen in Fig. 3A, for each sample, an asymmetrical Mn 2p_{3/2} peak located at 642.0 eV was observed. This peak could be deconvoluted into two components with a binding

energy of 641.5 and 642.8 eV, respectively. The former component was assigned to the Mn³⁺ ions whereas the latter one was attributed to the Mn⁴⁺ ions, indicating that Mn⁴⁺ and Mn³⁺ ions coexisted in all samples [28,29]. The concentration of Mn⁴⁺ on catalyst surface was obtained by quantitative analysis of the XPS spectra and is given in Table 3. The Ce and Mg substituted samples showed higher Mn⁴⁺ concentration and the Sr substituted sample had the lowest one. In Fig. 3B, the O 1s spectra were deconvoluted into three components at 529.3–529.5 eV, 531.0 eV and 532.5–532.7 eV referring to the surface lattice oxygen (denoted as O_α), surface adsorbed oxygen and some oxygen-containing groups such as OH[−] or CO₃^{2−} (denoted as O_β) and oxygen in surface adsorbed water molecules (denoted as O_γ), respectively [30–33]. From the calculated O_β/O molar ratio in Table 3, the O_β concentration of the LCMO

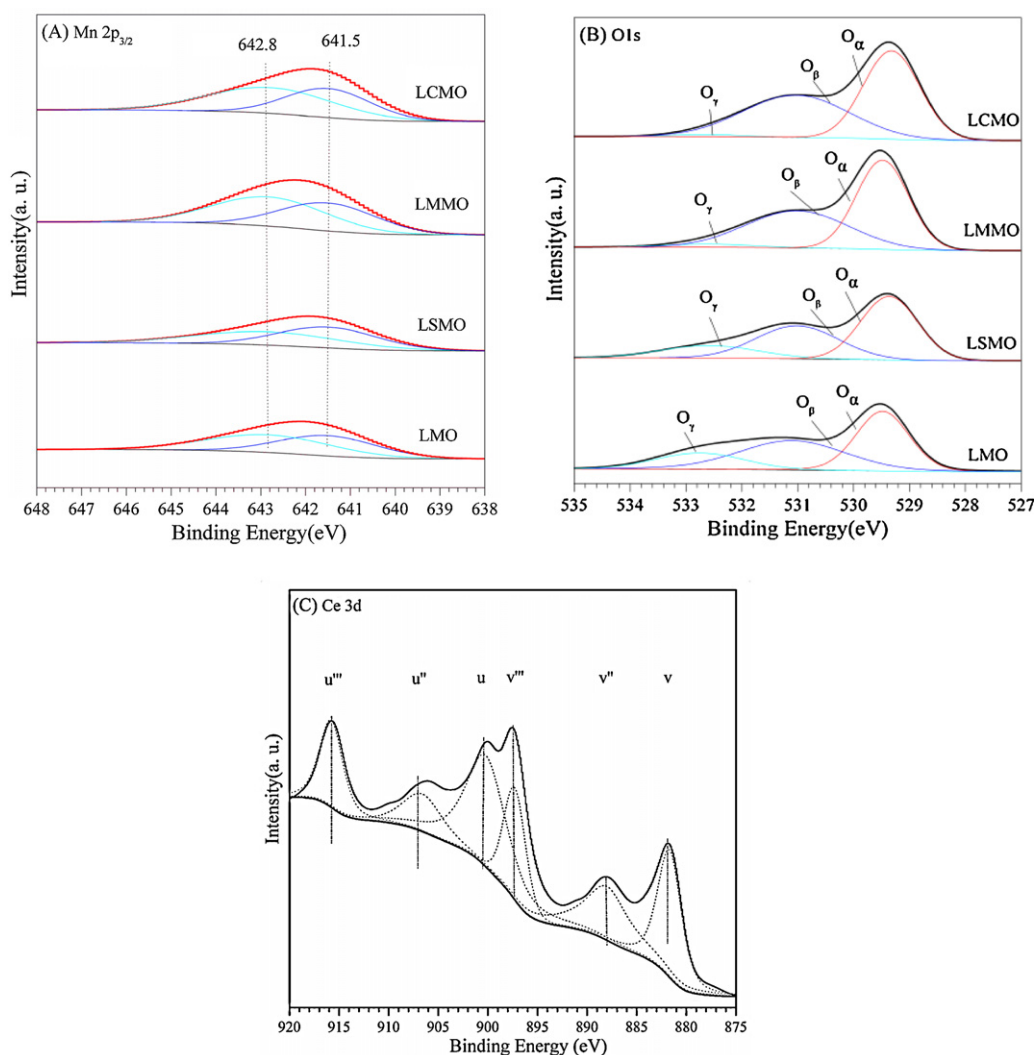


Fig. 3. (A) Mn 2p_{3/2}, (B) O 1s XPS spectra of LaMnO_3 and $\text{La}_{0.8}\text{A}_{0.2}\text{MnO}_3$ (A = Sr, Mg and Ce) catalysts and (C) Ce 3d XPS spectrum of $\text{La}_{0.8}\text{Ce}_{0.2}\text{MnO}_3$ catalyst.

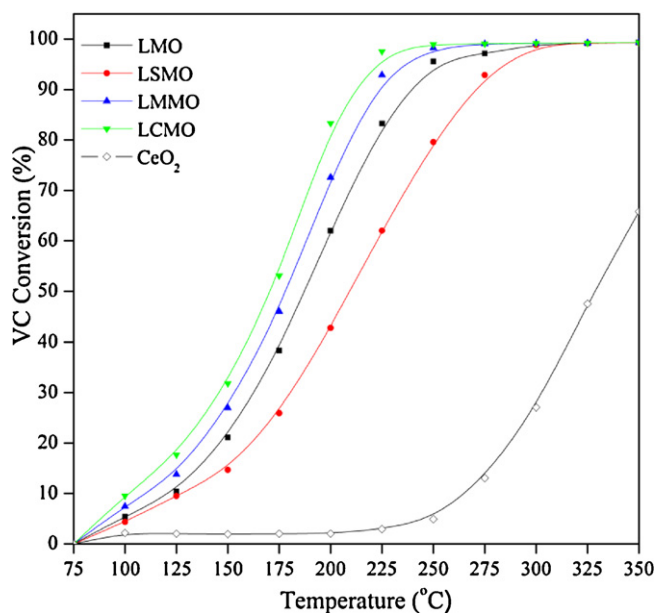


Fig. 4. VC conversion as a function of reaction temperature over LaMnO_3 and $\text{La}_{0.8}\text{A}_{0.2}\text{MnO}_3$ (A = Sr, Mg and Ce) catalysts.

sample was higher than those of any other samples. In addition, the LMMO sample also had higher O_β/O molar ratio than the LMO sample. However, the O_β concentration of the LSMO sample was the lowest. The ranking in terms of O_β/O molar ratio was in good agreement with the ranking observed for H_2 -TPR in the temperature range below 250 °C. More specifically for the LCMO sample, there was some accessional cerium oxide. Thus, it was greatly significant to find out the various oxidation states of cerium in this sample. As reported, it was very difficult to make an interpretation of the Ce 3d XPS spectrum due to the presence of more than 10 peak-contributions, correlated to the various oxidation states and multielectric splitting effect [34–36]. Even under some situations, the fine distinction of binding energy made the overlapped peaks assigned to various cerium species. In this work, only the obviously detected peaks were selected, marked, and discussed. As shown in Fig. 3C, the Ce 3d spectrum was composed of two multiplets (u and v), corresponding to the spin-orbit split $3d_{3/2}$ and $3d_{5/2}$ core holes. The spin-orbit splitting was about 18.6 eV, and each spin-orbit component was dominated by three features. It can be observed that the satellite peak u''' , located at about 915.8 eV, was the characteristic feature due to the presence of tetravalent Ce (Ce^{4+} ions) in the Ce compounds [37,38]. Besides, the highest binding energy peak v''' , located at about 897.3 ± 0.1 eV, the lower binding energy peaks u'' , v'' , u and v , respectively located at 906.6, 888.0, 900.2 and 881.7 eV, could be all attributed to Ce^{4+} with different electron configuration states [39]. It was concluded that Ce^{4+} was the dominant species in the LCMO sample, which was due to the good stability of Ce^{4+} at high calcination temperature.

3.4. Catalytic Activity

Fig. 4 shows the conversion of VC as a function of the reaction temperature over LaMnO_3 and $\text{La}_{0.8}\text{A}_{0.2}\text{MnO}_3$ (A = Sr, Mg and Ce) catalysts. Under the reaction conditions (VC concentration = 1000 ppm; GHSV = $15,000 \text{ h}^{-1}$), VC conversion increased gradually with the reaction temperature rise and VC was completely oxidized over all samples below 300 °C. During the VC oxidation process, an online INFICON IPC400 quadrupole mass spectrometer was used to identify the reaction products, indicating that only HCl, CO_2 and H_2O were finally produced and

there was no signal of byproducts such as chlorohydrocarbons and chlorine detected. It is common to evaluate and compare the catalytic activity of samples based on the T_{50} and T_{90} , which is the temperature corresponding to the 50% and 90% of VC conversion, respectively. The Ce-substituted sample LCMO exhibited the best catalytic activity for VC oxidation. The T_{50} and T_{90} values were 170 and 213 °C, respectively, which were 18 and 27 °C lower than those observed over the unsubstituted sample LMO ($T_{50} = 188$ °C and $T_{90} = 240$ °C). Similarly, an enhancement of the catalytic activity was also achieved by the substitution of La by Mg. Indeed, the overall activity curve of the LMMO sample shifted toward lower temperature compared with that of the LMO sample. Contrarily, an activity lose was observed for VC oxidation over the LSMO sample, indicating that the substitution of Sr had a negative effect on the catalytic performance of LaMnO_3 catalyst. Particularly for the LCMO sample, the influence of CeO_2 species on the catalytic activity should not be ignored. In order to make a comparison, a CeO_2 sample ($\text{SSA} = 54.9 \text{ m}^2 \text{ g}^{-1}$) was prepared by the same co-precipitation method with the calcination at 750 °C for 2 h and evaluated for the catalytic oxidation of VC under the same reaction conditions. As shown in Fig. 4, the CeO_2 sample exhibited extremely poor catalytic activity for this reaction. In the temperature range of 75–265 °C, the VC conversion remained less than 10%. Even at 300 °C, only 27% of VC was partially converted whereas a complete conversion was achieved over all perovskite samples at the same reaction temperature. The result indicated that, for the LCMO sample, the total activity could be attributed to the manganese perovskite phases and the active oxygen species. However, in the viewpoint that the cerium oxide exhibited poor catalytic activity for VC oxidation, cerium species made less contribution to the total catalytic performance of the LCMO sample. On the contrary, the perovskite oxide played an outstanding role in the catalytic oxidation of VC.

It has been reported that specific surface area, B-site cation reducibility and available oxygen species on the surface were the key factors to influence the oxidation activity of perovskite catalysts [6,9]. In order to investigate the internal relationship between these parameters and catalytic activity, a comprehensive analysis was made based on the results of catalyst characterizations and catalytic activity tests. It was found that the samples of LCMO and LMMO with SSA of 35.5 and $30.6 \text{ m}^2 \text{ g}^{-1}$, respectively, exhibited higher catalytic activity than LMO and LSMO (SSA around $16 \text{ m}^2 \text{ g}^{-1}$) samples for VC oxidation. Meanwhile, to assume that the increased SSA could improve the catalytic performance, the synthesis of the same perovskites with different SSA could be necessary. In addition, the substitution of Sr, Mg and Ce in the A-site had an effect on the surface Mn^{4+} concentration and on the amount of surface adsorbed oxygen species. It was revealed that the sample with the highest Mn^{4+}/Mn and O_β/O molar ratios also exhibited an outperforming performance for VC oxidation. The catalytic improvement could be explained by the fact that (i) the higher Mn^{4+}/Mn ratio could result in a higher average oxidation state of manganese, increase the crystal defects and generate more oxygen vacancies, leading to an enhanced redox property and oxygen mobility; (ii) the low temperature reducibility of the main redox couple of $\text{Mn}^{4+}/\text{Mn}^{3+}$ could also be improved by the higher Mn^{4+} concentration in the perovskite samples, speeding the redox cycles on/in the catalysts and (iii) as the most active oxygen species, surface adsorbed oxygen play a key role in the low temperature oxidation reaction [40,41]. The higher O_β/O ratio inferred that more surface adsorbed oxygen species were available and participated in the oxidation reaction of VC.

4. Conclusions

The LaMnO_3 and $\text{La}_{0.8}\text{A}_{0.2}\text{MnO}_3$ (A = Sr, Mg and Ce) perovskite-type oxides were prepared by co-precipitation method. The effect

of A-site substitution of the LaMnO_3 perovskite for vinyl chloride abatement was investigated. The substitution of Mg and Ce showed a positive effect on the catalytic performance for VC oxidation, but a negative effect was induced by the substitution of Sr cation. Among all samples, $\text{La}_{0.8}\text{Ce}_{0.2}\text{MnO}_3$ exhibited the best catalytic performance for VC oxidation with T_{50} of 170°C and T_{90} of 213°C . Higher specific surface area and more available adsorbed oxygen species on the surface should be mainly responsible for the remarkable enhancement of the catalytic activity. Furthermore, a higher average oxidation state of manganese was achieved by the substitution of Mg and Ce, resulting in an improved redox ability of the $\text{Mn}^{4+}/\text{Mn}^{3+}$ redox couple as well as the increase of the oxygen vacancies in the perovskite oxides.

Acknowledgement

This work was financially supported by the National Basic Research Program of China (2010CB732300), the National High Technology Research and Development Program of China (2011AA03A406) and 111 Project (B08021). The authors gratefully acknowledge the China Scholarship Council for the Joint-Training Scholarship Program with Institut de recherches sur la catalyse et l'environnement de Lyon (IRCELYON) and the Université Claude Bernard Lyon 1 (UCBL1).

References

- [1] F.I. Khan, A.K. Ghoshal, *Journal of Loss Prevention in the Process Industries* 13 (2000) 527–545.
- [2] K. Everaert, J. Baeyens, *Journal of Hazardous Materials* 109 (2004) 113–139.
- [3] M. Romero-Sáez, J.R. González-Velasco, M. Guillemot, P. Magnoux, *Applied Catalysis B* 88 (2009) 533–541.
- [4] I. Maupin, L. Pinard, J. Mijoin, P. Magnoux, *Journal of Catalysis* 291 (2012) 104–109.
- [5] R. Ma, P. Hu, L. Jin, Y. Wang, J. Lu, M. Luo, *Catalysis Today* 175 (2011) 598–602.
- [6] Y. Liu, H. Dai, Y. Du, J. Deng, L. Zhang, Z. Zhao, C.T. Au, *Journal of Catalysis* 287 (2012) 149–160.
- [7] M. Zawadzki, J. Trawczyński, *Catalysis Today* 176 (2011) 449–452.
- [8] C. Liang, C. Ku, Y. Chen, J. Liang, *Catalysis Communication* 17 (2012) 43–48.
- [9] V. Szabo, M. Bassir, A. Van Neste, S. Kaliaguine, *Applied Catalysis B* 37 (2002) 175–180.
- [10] B. Levasseur, S. Kaliaguine, *Journal of Solid State Chemistry* 181 (2008) 2953–2963.
- [11] M.C. Álvarez-Galvina, V.A. de la Peña O'Sheab, G. Arzamendic, B. Paweleca, L.M. Gandía, J.L.G. Fierro, *Applied Catalysis B* 92 (2009) 445–453.
- [12] D.D. Agarwal, H.S. Goswami, *Reaction Kinetics and Catalysis Letters* 53 (1994) 441–449.
- [13] N.A. Merino, B.P. Barbero, P. Ruiz, L.E. Cadús, *Journal of Catalysis* 240 (2006) 245–257.
- [14] H. Taguchi, K. Matsu-ur, M. Takada, K. Hirot, *Journal of Solid State Chemistry* 190 (2012) 157–161.
- [15] K. Rida, A. Benabbas, F. Bouremmad, M.A. Peña, A. Martínez-Arias, *Catalysis Communication* 7 (2006) 963–968.
- [16] N.A. Merino, B.P. Barbero, P. Grange, L.E. Cadús, *Journal of Catalysis* 231 (2005) 232–244.
- [17] B. Levasseur, S. Kaliaguine, *Applied Catalysis B* 88 (2009) 305–314.
- [18] C. Zhang, C. Wang, W. Zhan, Y. Guo, Y. Guo, G. Lu, A. Baylet, A. Giroir-Fendler, *Applied Catalysis B* 129 (2013) 509–516.
- [19] J.A. Alonso, M.J. Martínez-Lope, M.T. Casais, J.L. MacManus-Driscoll, P.S.I.P.N. de Silva, L.F. Cohen, M.T. Fernández-díza, *Journal of Materials Chemistry* 7 (1997) 2139–2144.
- [20] B. He, Q. Song, Q. Yao, Z. Meng, C. Chen, *Korean Journal of Chemical Engineering* 24 (2007) 503–507.
- [21] E. Aneggi, C. de Leitenburg, A. Trovarelli, *Catalysis Today* 181 (2012) 108–115.
- [22] S. Irueta, M.P. Pina, M. Menéndez, J. Santamaria, *Journal of Catalysis* 179 (1998) 400–412.
- [23] A. Kaddouri, S. Ifra, *Catalysis Communication* 7 (2006) 109–113.
- [24] S.M. Lima, J.M. Assaf, M.A. Peña, J.L.G. Fierro, *Applied Catalysis A* 311 (2006) 94–104.
- [25] A. Kaddouri, P. Gelin, N. Dupont, *Catalysis Communication* 10 (2009) 1085–1089.
- [26] M. Alifanti, J. Kirchnerova, B. Delmon, *Applied Catalysis A* 245 (2003) 231–243.
- [27] R. Hammami, S.B. Aïssa, H. Batis, *Applied Catalysis A* 353 (2009) 145–153.
- [28] S. Ponce, M.A. Peña, J.L.G. Fierro, *Applied Catalysis B* 24 (2000) 193–205.
- [29] J. Deng, L. Zhang, H. Dai, H. He, C.T. Au, *Industrial & Engineering Chemistry Research* 47 (2008) 8175–8183.
- [30] J.L.G. Fierro, L. Gonzalez Tejuca, *Applied Surface Science* 27 (1987) 453–457.
- [31] A.F. Carley, M.W. Roberts, A.K. Santra, *The Journal of Physical Chemistry B* 101 (1997) 9978–9983.
- [32] M.M. Natile, E. Ugel, C. Maccato, A. Glisenti, *Applied Catalysis B* 72 (2007) 351–362.
- [33] S. Kaliaguine, A. Van Neste, V. Szabo, J.E. Gallot, M. Bassir, R. Muzychuk, *Applied Catalysis A* 209 (2001) 345–358.
- [34] J.G. Numan, H. Robota, M. Cohn, S. Bradley, *Journal of Catalysis* 133 (1992) 309–324.
- [35] K.-D. Schierbaum, *Surface Science* 399 (1998) 29–38.
- [36] A. Baylet, C. Capdeillayre, L. Retailleau, P. Vernoux, F. Figueras, A. Giroir-Fendler, *Applied Catalysis B* 96 (2010) 434–440.
- [37] J.Z. Shyu, K. Otto, *Journal of Catalysis* 115 (1989) 16–23.
- [38] M. Romeo, K. Bak, J. El Fallah, F. Le Normand, L. Hilaire, *Surface and Interface Analysis* 20 (1993) 508–512.
- [39] E. Bêche, P. Charvin, D. Perarnau, S. Abanades, G. Flamant, *Surface and Interface Analysis* 40 (2008) 264–267.
- [40] Z. Wei, L. Wei, L. Gong, Y. Wang, C. Hu, *Journal of Hazardous Materials* 177 (2010) 554–559.
- [41] C. Li, Y. Lin, *Applied Catalysis B* 107 (2011) 284–293.